



CHORUS

This is the accepted manuscript made available via CHORUS. The article has been published as:

Decoherence and spin echo in biological systems

Alexander I. Nesterov and Gennady P. Berman

Phys. Rev. E **91**, 052702 — Published 7 May 2015

DOI: [10.1103/PhysRevE.91.052702](https://doi.org/10.1103/PhysRevE.91.052702)

On Decoherence and Spin Echo in Biological Systems

Alexander I. Nesterov*

*Departamento de Física, CUCEI, Universidad de Guadalajara,
Av. Revolución 1500, Guadalajara, CP 44420, Jalisco, México*

Gennady P. Berman†

*Theoretical Division, T-4, Los Alamos National Laboratory,
and the New Mexico Consortium, Los Alamos, NM 87544, USA*

The spin echo approach is extended to include bio-complexes for which the interaction with dynamical noise, produced by the protein environment, is strong. Significant restoration of the free induction decay signal due to homogeneous (decoherence) and inhomogeneous (dephasing) broadening is demonstrated analytically and numerically, for both an individual dimer of interacting chlorophylls and for an ensemble of dimers. Our approach does not require the use of small interaction constants between the electron states and the protein fluctuations. It is based on an exact and closed system of ordinary differential equations that can be easily solved for a wide range of parameters that are relevant for bio-applications.

PACS numbers: 03.65.Yz, 87.18.Tt, 82.53.Ps

Keywords: Decoherence, noise, spin echo

I. INTRODUCTION

The spectroscopic and measuring technologies, developed during last few decades, have allowed experimental scientists to examine very rapid dynamical processes, including those in biological systems. One of them is the very powerful 2D femtosecond *nonlinear* spectroscopy, which is a special case of parametric four-wave mixing, in which three pulses interact with the system to produce a signal field in a particular phase-matched direction. In this case, the 2D frequency spectra at different delay times is used to recover the dynamics of the electron population between different sites of the bio-complexes, and estimate the characteristic decoherence time in these systems (time-decay of the non-diagonal elements of the density matrix) [1]. In particular, it was demonstrated that, even at room temperature, photosynthetic bio-complexes exhibit collective quantum coherence (CQC) during primary electron transfer (ET) processes that occur on the time-scale of some hundreds of femtoseconds [1]. The CQC is resulted from the fact that the primary processes of exciton transfer and charge separation are so rapid (on a time-scale of a few picoseconds) that the protein environment does not have time to recombine the exciton and destroy the CQC. In [2], the integrated

two-color coherence photon echo (2CCPE) approach, based on the 2D femtosecond nonlinear spectroscopy, was used to partly suppress the inhomogeneous broadening of excitonic coherence in a strongly coupled dimer system, such as the bacteriopheophytinbacteriochlorophyll pair in the bacterial reaction center. In particular, the authors of [2] demonstrated that beside the ensemble dephasing, the coherence in such a system exhibits a bi-exponential decay with a slow component with a lifetime of hundreds of femtoseconds and a rapid component with a lifetime of tens of femtoseconds.

The optical spin echo spectroscopy is a modification of the well-known approach which was initially developed in the nuclear magnetic resonance [3, 4]. This Hahn spin echo spectroscopy (HSES) is a *linear* approach, which allows one to reduce the effects of the “inhomogeneous broadening” (dephasing) in an ensemble of spins and to increase the time of the signal generated by the transverse magnetization (free induction, FI).

The important development of the HSES during the last decade was the recognition that it can be successfully applied not only to an ensemble of effective spins, but also to an individual spin, or to an individual two-level quantum system (TLS) [5]. In this case, inhomogeneous broadening is absent. But still one can partly suppress the broadening of the FI decay resulted from a pure dynamical (time-dependent) noise. In [5–8] the HSES was applied to a single quantum two-level system - the superconducting qubit. In this case, the qubit is considered

*Electronic address: nesterov@cencar.udg.mx

†Electronic address: gpb@lanl.gov

in the so-called diagonal representation, with the main characteristic being the energy gap (usually tens of gigahertz) between the ground and the excited states. The dynamical noise, acting on the qubit, is generated by the time-fluctuations of the electron charge, bias current, external magnetic flux, and other sources. All these sources of noise for superconducting qubits are relatively weak, so the perturbation approaches can be used.

In contrast to a superconducting qubit, an individual effective two-level quantum system (a dimer) in a bio-complex is usually characterized in the so-called site representation, using such main parameters as the energy gap (redox potential) between the excited states of the chlorophylls realizing this dimer, and the matrix element of the dipole-dipole or the exchange interactions between these two excited states. Also, the dimer usually experiences a strong interaction with the protein fluctuations (characterized by the reconstruction energy), caused by dynamical noise, that must be taken into account in bio-applications of the spin echo spectroscopy.

In this paper, we analyze analytically and numerically the application of the HSES for both an individual dimer and for an ensemble of dimers in bio-complexes, for the case of strong interaction with the protein environment. In our model, a single dimer in the light-harvesting complex (LHC) is composed of the excited states, $|1\rangle$ and $|2\rangle$, of two chlorophylls, Chl1 (donor) and Chl2 (acceptor). If, for example, initially the donor is populated, the energy (exciton) can be transferred to the acceptor due to (i) the interaction of the transitional dipole moments of two chlorophylls, which is characterized by the matrix element, V_{12} (time-reversal dynamics), and (ii) the Coulomb interactions between the electron in the states $|1\rangle$ and $|2\rangle$ and the protein fluctuations. (The environment-assisted energy transfer [9].) Usually, the protein fluctuations are modeled by the ensemble of quantum harmonic oscillators of nuclear degrees of freedom, or by the corresponding bosonic electromagnetic modes. (See [9–11], and references therein.) Also, some different models for the protein fluctuations are used based on (i) an external noise [12–15] and (ii) the hybrid approaches [16]. For our purposes, we assume that the dimer experiences the influence of a stochastic process (noise) from the protein environment, which is characterized by two parameters: (i) the amplitude of noise and (ii) the decay rate (or correlation time) of the noise correlation function (non-

Markovian approximation). This approximation corresponds to the “infinite temperature” regime, and reasonably describes the Coulomb interaction of the electron in the excited states of the chlorophyll molecules with the electromagnetic protein fluctuations, if one is interested in the fast electron transfer dynamics, and is not interested in the temperature dependences of the electron transfer rates.

We recognize that the application of the linear HSES may not be the optimal realization of the spin echo protocols in the optical domain. At the same time, the main effects, discussed in this paper, can easily be demonstrated by using a simple HSES, with possible further generalizations for more complex protocols used in the optical applications.

We show that both the dynamical and the inhomogeneous broadening of the FI decay can be successfully suppressed by the spin echo pulses, in a wide range of parameters. Our conclusion is that (i) even for strong interaction with the dynamical noise and (ii) in the presence of relaxation (transverse noise), the spin echo spectroscopy can serve as the useful complementary spectroscopic technique for characterizing the bio-complexes that include both individual dimers and an ensemble of dimers.

The important advantage of our approach is that it is based on the exact and closed system of ordinary linear differential equations with constant coefficients, which we derived for time-dependent observable variables. So, our approach does not use the approximations like small interaction constants with protein environment. In particular, our approach includes the results which followed from the well-known Bloch-Redfield theory [17–19] as a limited case.

The structure of the paper is the following. In Section II, we introduce the model and derive the closed system of differential equations for the averaged Bloch vector. In Section III, we apply our approach to describe homogeneous broadening due to dynamical noise, and present the results of the numerical simulations for both exact and approximate solutions. In Section III, we consider simultaneous action of the homogeneous and inhomogeneous disorder. In the Conclusion, we summarize our results and formulate some challenges for future research.

II. DESCRIPTION OF THE MODEL

First, consider a single dimer in the LHC composed of the excited states, $|1\rangle$ and $|2\rangle$,

of two chlorophylls, Chl1 (donor) and Chl2 (acceptor), interacting through the matrix element, V_{12} (see above). We assume that each chlorophyll experiences a diagonal noise (see [10, 11] for details), provided by the protein environment, which is described by the random variable, $\xi(t)$. Similar to the Coulomb interaction of the excited electron in the dimer with the different electromagnetic modes of the thermal protein environment, in our model the same electron interacts with the electromagnetic modes provided by noisy protein fluctuations which are characterized by two parameters: (i) the amplitude and (ii) the decay rate of the correlation function. Usually, the protein noise is also characterized by the corresponding spectral density of noise, $S(\omega)$, where ω is the frequency of the noisy component. The interactions between the protein noise and the two dimer states are characterized by two interaction constants, $\lambda_{1,2}$, which usually are not small in bio-systems at ambient conditions.

In the site (donor-acceptor) representation, the Hamiltonian of the system can be written as follows: $\mathcal{H} = E_1|1\rangle\langle 1| + E_2|2\rangle\langle 2| + (1/2)(V_{12}|1\rangle\langle 2| + h.c.) + \xi(t)(\lambda_1|1\rangle\langle 1| + \lambda_2|2\rangle\langle 2|)$.

We assume that noise is produced by the stationary random telegraph process (RTP) with: $\langle \xi(t) \rangle = 0$, $\langle \xi(t)\xi(t') \rangle = \chi(t-t')$, where, $\chi(t-t') = \sigma^2 e^{-2\gamma|t-t'|}$, is the correlation function; σ , 2γ , and $\lambda_{1,2}$, are the amplitude of noise, the decay rate of the correlation function, and the interaction constants with noise, correspondingly.

In the diagonal representation of the unperturbed Hamiltonian, we obtain the total Hamiltonian for the effective TLS,

$$\mathcal{H} = \frac{\lambda_0}{2}I + \frac{1}{2}\Omega\sigma_z + \frac{1}{2}D_{\lambda,z}\xi(t)\sigma_z + \frac{1}{2}D_{\lambda,\perp}\xi(t)(\cos\phi\sigma_x + \sin\phi\sigma_y), \quad (1)$$

where, $\sigma_{x,y,z}$, are the Pauli matrices, $\lambda_0 = E_1 + E_2 + (\lambda_1 + \lambda_2)\xi(t)$, $\lambda = \lambda_1 - \lambda_2$, $\Omega = \sqrt{(E_1 - E_2)^2 + |V_{12}|^2}$, $D_{\lambda,z} = \lambda \cos\theta$, and $D_{\lambda,\perp} = \lambda \sin\theta$. We set: $V_{12} = |V_{12}|e^{-i\phi}$, and $\cos\theta = (E_1 - E_2)/\Omega$.

The Bloch-Redfield approximation

The dynamics of a TLS is described by two rates: the longitudinal relaxation rate, $\Gamma_1 = T_1^{-1}$, and the transverse relaxation rate, $\Gamma_2 = T_2^{-1}$. When the noise is weak, and the condition, $\tau_c \ll T_1, T_2$, is satisfied (where $\tau_c =$

$1/(2\gamma)$ is the correlation time of the noise fluctuations), one can apply Bloch-Redfield (BR) theory [17–19]. In BR theory, the transverse relaxation rate, $\Gamma_2 = \Gamma_\varphi + \Gamma_1/2$, where Γ_φ is the so-called “dephasing” rate. (For a single dimer, Γ_2 is the decoherence rate.) In terms of the spectral density of noise, $S(\omega)$, these rates are defined as follows [5]: $\Gamma_1 = \pi D_{\lambda,\perp}^2 S(\Omega)$, $\Gamma_\varphi = \pi D_{\lambda,z}^2 S(0)$. Using the spectral density of RTP, $S(\omega) = 2\gamma\sigma^2/\pi(4\gamma^2 + \omega^2)$, we obtain the relaxation and dephasing rates provided by BR theory: $\Gamma_1 = 2\gamma v^2 \sin^2\theta/(4\gamma^2 + \Omega^2)$, $\Gamma_\varphi = (v^2/2\gamma) \cos^2\theta$, where the renormalized interaction constant with noise, $v = \lambda\sigma$, is introduced.

A. The generalized approach based on the exact equations

To study the quantum decoherence and relaxation processes in general case, we present the density matrix as, $\rho(t) = (I + \mathbf{n}(t) \cdot \boldsymbol{\sigma})/2$, where, $\mathbf{n}(t) = \text{Tr}(\rho(t)\boldsymbol{\sigma})$, is the Bloch vector. Instead of the Liouville-von Neumann equation for the density matrix, $i\hbar\dot{\rho} = [\mathcal{H}, \rho]$, it is convenient to employ the equation of motion for the Bloch vector (we set $\hbar = 1$):

$$\frac{d\mathbf{n}}{dt} = \boldsymbol{\Omega} \times \mathbf{n} + (\xi(t)/\sigma)\boldsymbol{\omega} \times \mathbf{n}. \quad (2)$$

Here the vector, $\boldsymbol{\omega} = v(\sin\theta \cos\phi, \sin\theta \sin\phi, \cos\theta)$, characterizes the interaction with noise, and $\boldsymbol{\Omega} = (0, 0, \Omega)$ is the effective external field, which in the diagonal representation is oriented in the z -direction. It is important to note that the introduced above density matrix, $\rho(t)$, and the Bloch vector in Eq. (2) depend on a concrete realization of the random process, $\xi(t)$.

Using the differential formula for the RTP [20],

$$\left(\frac{d}{dt} + 2\gamma\right)\langle \xi(t)R[t; \xi(\tau)] \rangle = \left\langle \xi(t) \frac{d}{dt} R[t; \xi(\tau)] \right\rangle, \quad (3)$$

where, $R[t; \xi(\tau)]$, is an arbitrary functional, we obtain from Eq. (2) the closed system of differential equations:

$$\frac{d\langle \mathbf{n} \rangle}{dt} = \boldsymbol{\Omega} \times \langle \mathbf{n} \rangle + \boldsymbol{\omega} \times \langle \mathbf{n}^\xi \rangle, \quad (4)$$

$$\frac{d\langle \mathbf{n}^\xi \rangle}{dt} = \boldsymbol{\Omega} \times \langle \mathbf{n}^\xi \rangle + \boldsymbol{\omega} \times \langle \mathbf{n} \rangle - 2\gamma\langle \mathbf{n}^\xi \rangle, \quad (5)$$

where, $\langle \mathbf{n}^\xi \rangle = \langle \xi(t) \mathbf{n} \rangle / \sigma$. The average, $\langle \dots \rangle$, is taken over the RTP. Below, when presenting

the analytical expressions and the results of numerical simulations, we are dealing only with the averaged over noise Bloch vector, $\langle \mathbf{n}(t) \rangle$, and other time-dependent expressions.

Weakly and strongly coupled dimers. To characterize a dimer, we introduce the dimensionless parameter, $\epsilon = |\tan \theta| = |V_{12}/(E_1 - E_2)|$. When $\epsilon \ll 1$, we will call the dimer “weakly coupled”. In the opposite case, $\epsilon \gtrsim 1$, the dimer is called “strongly coupled”.

Scaling properties. For a weakly coupled dimer, one can use the following approximation in Eqs. (4) and (5): $\boldsymbol{\omega} \approx v(0, 0, 1)$. Let us assume that the external resonance field (a pulse), $\boldsymbol{\Omega}_R = \Omega_R(\cos(\Omega t), \sin(\Omega t), 0)$, is applied in the (xy) -plane to the TLS, where the frequency of the external field is: $\Omega_{ext} = \Omega$, and Ω_R is the amplitude of the field (the Rabi frequency). Then, in the reference frame rotating with the frequency, Ω , the equations of motion can be written as,

$$\begin{aligned} \frac{d\langle \mathbf{n}_R \rangle}{dt} &= \boldsymbol{\Omega}_R \times \langle \mathbf{n}_R \rangle + \boldsymbol{\omega} \times \langle \mathbf{n}_R^\xi \rangle, \\ \frac{d\langle \mathbf{n}_R^\xi \rangle}{dt} &= \boldsymbol{\Omega}_R \times \langle \mathbf{n}_R^\xi \rangle + \boldsymbol{\omega} \times \langle \mathbf{n}_R \rangle - 2\gamma \langle \mathbf{n}_R^\xi \rangle. \end{aligned} \quad (6)$$

$$(7)$$

From here it follows that the TLS has a scaling invariance with respect to the transformation of time: $t \rightarrow \alpha t$, if we rescale the parameters of the system as follows: $\Omega_R \rightarrow \alpha^{-1}\Omega_R$, $v \rightarrow \alpha^{-1}v$, and $\gamma \rightarrow \alpha^{-1}\gamma$, where α is an arbitrary constant.

III. HOMOGENEOUS BROADENING DUE TO DYNAMICAL NOISE

It is well-known that the main contribution to the decoherence (or dephasing) time of an individual TLS (or an ensemble of TLSs) is due to the fluctuations of the “longitudinal effective magnetic field”, which in our case of Eq. (1) is proportional to $D_{\lambda,z}$. Correspondingly, the amplitude of fluctuations of the “transverse effective magnetic field” is proportional to $D_{\lambda,\perp}$. Below, we will mainly be interested in the characteristic time of the FI decay, and how the Hahn spin echo pulses influence this process. Then, the main interest represents the case when the ratio of the amplitude of the transverse effective magnetic field to the amplitude of the longitudinal effective magnetic field is a small parameter: $|D_{\lambda,\perp}/D_{\lambda,z}| = |\tan \theta| = \epsilon \ll 1$, which also

corresponds to the case of a weakly coupled dimer. In this case, for an approximate analytical solution of Eqs. (4) and (5) one can neglect the effects of relaxation. Introducing the complex vectors: $\langle m(t) \rangle = \langle n_x(t) \rangle + i\langle n_y(t) \rangle$ and $\langle m^\xi(t) \rangle = \langle n_x^\xi(t) \rangle + i\langle n_y^\xi(t) \rangle$, one can show that the solution of Eqs. (4) and (5) can be written as,

$$\langle n_z(t) \rangle = \langle n_z(0) \rangle, \quad \langle n_z^\xi(t) \rangle = 0, \quad (8)$$

$$\langle m(t) \rangle = e^{i\Omega t} \Phi(t) \langle m(0) \rangle, \quad (9)$$

$$\langle m^\xi(t) \rangle = -\frac{ie^{i\Omega t}}{v \cos \theta} \frac{d\Phi(t)}{dt} \langle m(0) \rangle. \quad (10)$$

Here we denote by $\Phi(t)$ the generating functional of the RTP [20]. For the FI decay, it is given by [6–8],

$$\Phi^f(t) = e^{-\gamma t} \left(\frac{1}{\mu} \sinh(\gamma \mu t) + \cosh(\gamma \mu t) \right), \quad (11)$$

where, $\mu = \sqrt{1 - (v \cos \theta / \gamma)^2}$.

Below, we will compare the approximate analytical solution (8) - (10) with the numerical solution of the exact Eqs. (4) and (5). It will be demonstrated that a good coincidence of both these solutions extends even for a strongly coupled dimer ($\epsilon \sim 1$) and, consequently, for strong transverse noise.

We also would like to note that the results of our numerical simulations only weakly depend of the phase, ϕ , of the matrix element, V_{12} . So, in all cases presented below for individual dimers, we have chosen, $\phi = 0$.

A. Free induction signal decay

We call noise weak if the dimensionless parameter, $\eta = |v \cos \theta / \gamma| \ll 1$. The main reason for this is, that as it follows from Eq. (11), for weak noise, the decay rate of the non-diagonal averaged density matrix element (which characterizes the decoherence) coincides with Γ_φ , provided by BR-theory. We call noise strong if $\eta \gtrsim 1$. In particular, when $\eta > 1$, the parameter, μ in Eq. (11) becomes imaginary, and the decay of the functional, $\Phi^f(t)$, is accompanied by oscillations with frequency, $\gamma|\mu|$ (or the period: $T = 2\pi/\gamma|\mu|$).

Below, we compare the analytical solutions (8) - (10), when the transverse effective field (relaxation) is neglected, with the corresponding exact solutions obtained numerically from Eqs. (4) and (5). In numerical simulations, we put $\hbar = 1$. All energy-dimensional parameters

are measured in ps^{-1} ($1\text{ps}^{-1} \approx 0.66 \text{ meV}$), and time is measured in ps.

In Fig. 1, the strongly coupled dimer was considered ($\theta \approx 0.968$, $\epsilon \approx 1.45$). One can see, that in spite of the noise is strong: $\eta \approx 1.13$ (red dashed curve) and $\eta \approx 2.27$ (orange dashed curve), the approximate analytical solutions (shown by blue curves), are in a good agreement with the exact numerical solutions. In the inset, the noise amplitude is relatively large ($v = 20$), and the matrix element, V_{12} , of the Chl1 and Chl2 interaction, is also large: $\epsilon \approx 8.24$ (strongly coupled dimer). At the same time, the noise is weak: $\eta \approx 0.24$, and the BR approach works. However, one cannot neglect the contribution from the transverse field to the decoherence rate, $\Gamma_2 = \Gamma_\varphi + \Gamma_1/2$. Indeed, in this case, $\Gamma_\varphi \approx 0.3$ and $\Gamma_1 \approx 0.48$. That is why the approximate solution in the inset (blue curve) deviates significantly from the exact numerical solution (red dashed curve).

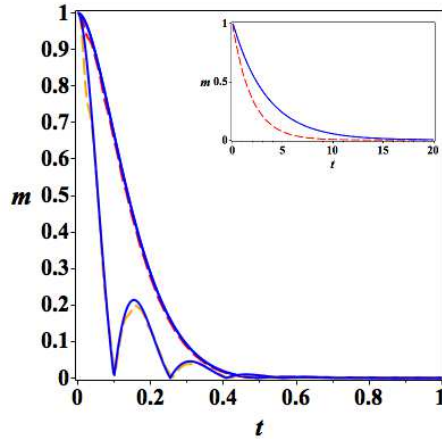


FIG. 1: (Color online) Time dependence (in ps) of $m = |\langle m(t) \rangle|$, for the FI signal. Blue curves: analytical results. Dashed curves: exact solution. Parameters: $\Omega = 127$, $\theta = 0.968$, $\gamma = 10$, $v = 20$ (red curve), $v = 40$ (orange curve). Inset: $\theta = 1.45$, $v = 20$.

B. Echo signal

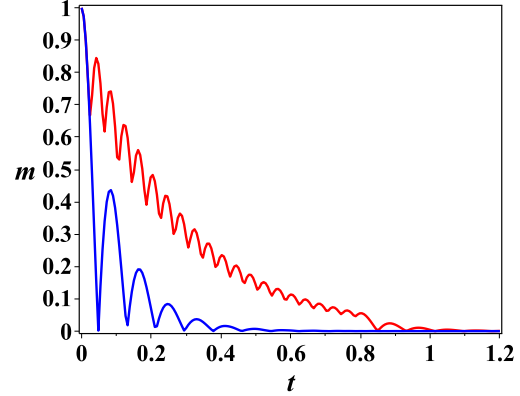
For simplicity, we assume in the analytical estimates that the spin echo π -pulses act practically instantaneously. The spin echo pulse, applied at the time τ , rotates the wave function around the x -axis, by the angle π . The corresponding analytical solution for the generating

functional can be written as,

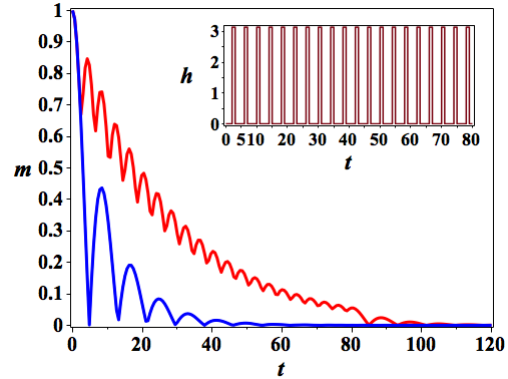
$$\Phi^e(t) = \begin{cases} \Phi^f(t), & 0 < t < \tau, \\ \Phi_g^f(t), & t > \tau, \end{cases} \quad (12)$$

where,

$$\begin{aligned} \Phi_g^f(t) = & \Phi^f(t) + e^{-\gamma t} \left(1 - \frac{1}{\mu^2}\right) (\cosh(\gamma\mu(t - 2\tau)) \\ & - \cosh(\gamma\mu t)). \end{aligned} \quad (13)$$



(a)



(b)

FIG. 2: (Color online) Time dependence (in ps) of $m = |\langle m(t) \rangle|$. The FI decay: blue curves. Echo signals: red curves. Number of echo pulses, $N = 20$. (a) Parameters: $\Omega = 150$, $v = 40$, $\gamma = 10$, $\theta = 0.165$. The duration of each pulse is: $\delta = 10 \text{ fs}$, and its height is: $h = 100\pi$. (b) Parameters: $\Omega = 150$, $v = 0.4$, $\gamma = 0.1$, $\theta = 0.165$. Inset: the sequence of π -pulses applied to the system. The duration of each pulse is: $\delta = 1\text{ps}$, and its height is: $h = \pi$.

Below, we demonstrate that our analytical solutions, given by Eqs. (8) – (10) and Eqs. (12), (13), are in a good agreement with the exact numerical solutions, up to the value of $\epsilon \approx 1.72$ ($\theta \lesssim \pi/3$) and for the finite width of the π -pulse (for example, $\delta = 1\text{ps}$), for both

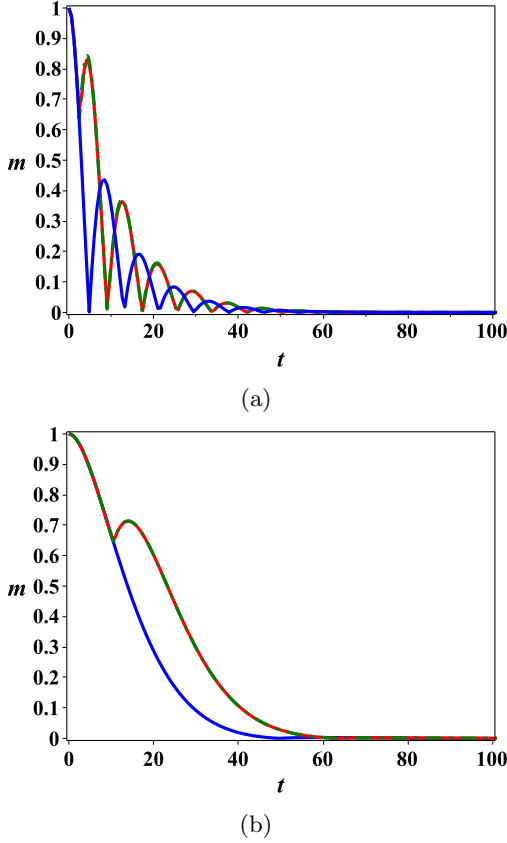


FIG. 3: (Color online) A comparison of analytical and numerical solutions. Time dependence (in ps) of $m = |\langle m(t) \rangle|$. Numerical solution: red curves. Analytical solution: green dashed curves. The FI decay: Blue curves. Parameters: (a) $\Omega = 150$, $v = 0.4$, $\gamma = 0.1$, $\theta = 0.165$, $\tau = 2.5$ ps; (b) $\Omega = 127$, $v = 0.2$, $\gamma = 0.1$, $\theta = 0.968$, $\tau = 10.5$ ps. The duration of the π -pulse is: $\delta = 1$ ps, and its height is: $h = \pi$.

weakly and strongly coupled dimers, and even for relatively large noise.

In the numerical simulations, we use the echo pulses of finite duration. We assume that the circular polarized field, $\mathbf{\Omega}_R(t) = \Omega_R(t)(\cos(\Omega t), \sin(\Omega t), 0)$, is applied after the FI decay, at time, τ . Here,

$$\Omega_R(t) = \begin{cases} 0, & 0 \leq t < \tau, \\ h, & \tau \leq t \leq \tau + \delta, \\ 0, & t > \tau + \delta. \end{cases} \quad (14)$$

The duration of this pulse is δ , and its amplitude, h , is found from the condition: $h\delta = \pi$.

In Fig. 2, the time dependence (in ps) of the transverse Bloch vector, $m(t) = |\langle m(t) \rangle|$, is shown. The FI decay corresponds to the blue curves. The spin echo signals correspond to the red curves. The number of echo pulses is,

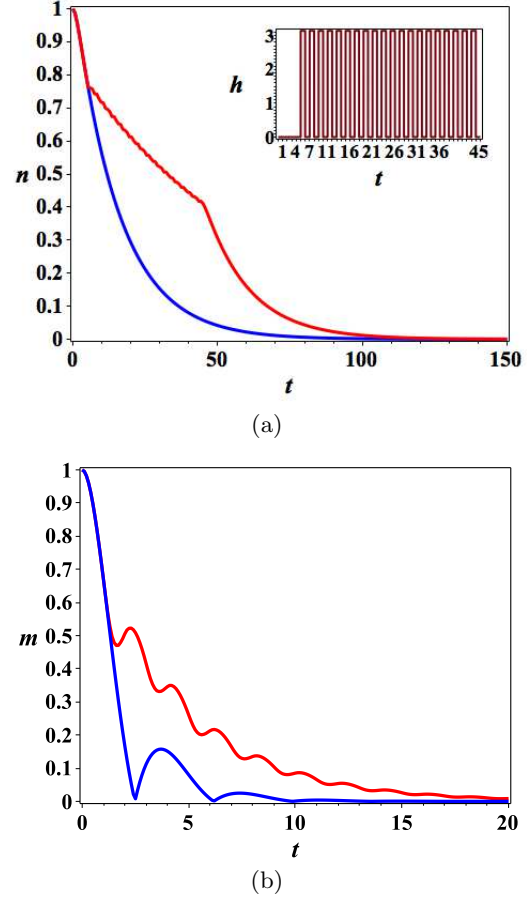


FIG. 4: (Color online) Time dependence (in ps) of $m = |\langle m(t) \rangle|$. The FI decay: blue curve. Echo signal: red curve. The duration of each echo π -pulse is: $\delta = 1$ ps, and its height is: $h = \pi$. Parameters: $\Omega = 150$, $\gamma = 0.5$, $\theta = 0.165$. (a) Number of pulses is: $N = 20$ ($v = 0.25$). Inset: the sequence of π -pulses applied to the system. (b) Number of pulses is: $N = 10$ ($v = 1$).

$N = 20$. Parameters in Fig. 2a were chosen: $\Omega = 150$, $v = 40$, $\gamma = 10$, $\theta = 0.165$. At $\tau = 20$ fs, the first π -pulse, with the width, $\delta = 10$ fs, was applied. The distance between π -pulses was chosen: $\Delta = 30$ fs. This case corresponds to a weakly coupled dimer ($\epsilon \approx 0.17$), and to strong noise: $\eta \approx 3.9$. The FI decay exhibits oscillations with the period: $T = 2\pi/\gamma|\mu| \approx 0.16$. Note, that the results with such a short π -pulse are presented here mainly for the purposes of illustration of the discussed in Sec. II A scaling effects. This kind of π -pulses require very large Rabi frequencies, and large values of the corresponding electric fields, which could destroy the system [21].

Parameters in Fig. 2b were chosen: $\Omega = 150$, $v = 0.4$, $\gamma = 0.1$, $\theta = 0.165$, $\tau = 2$ ps, $\delta = 1$ ps,

$\Delta = 3\text{ps}$. This case corresponds to a weakly coupled dimer ($\epsilon \approx 0.17$), and to strong noise: $\eta \approx 3.9$. The FI decay exhibits oscillations with the period: $T = 2\pi/\gamma|\mu| \approx 16.5$. (Note, that in Figs. 2, the modules of the transverse Bloch vector, $|\langle m(t) \rangle|$, is presented.) The inset shows the sequence of π -pulses applied to the system, with the duration of each pulse, $\delta = 1\text{ps}$, and $\Delta = 3\text{ps}$. As one can see by comparison of Fig. 2a and Fig. 2b, the scaling takes place, which was discussed in Sec. II A. One can also see from Figs. 2a and 2b that the homogeneous broadening of the FI signal can be significantly improved by applying the Hahn spin echo pulses.

In Figs. 3a and 3b, we compare our analytical solutions, given by Eqs. (8)–(10) and Eqs. (12), (13), with the exact numerical solutions of Eqs. (4) and (5) and Eqs. (6) and (7). In analytical solutions the π -pulse was applied at the middle of the π -pulse of the corresponding numerical solutions. In Fig. 3a, a weakly coupled dimer is considered ($\epsilon \approx 0.17$), and the noise is strong ($\eta \approx 3.9$). Initially, the Bloch vector was positioned in the x -direction. The red curve demonstrates the results of the exact numerical simulations. During the time, $\tau = 2.5\text{ps}$, the Bloch vector experiences the FI decay. At time, $t = 2.5\text{ps}$, the π -pulse was applied of the duration, $\delta = 1\text{ps}$. After the end of the π -pulse, the Bloch vector experiences the FI decay. The green dashed curve describes the corresponding analytical solution. As one can see, both solutions practically coincide. The blue curve corresponds to the FI decay. All solutions oscillate, as the values of parameter, μ , in Eq. (11) are imaginary. In Fig. 3b, a strongly coupled dimer is considered ($\epsilon \approx 1.45$), and the noise is strong ($\eta \approx 1.1$). The π -pulse of duration, $\delta = 1\text{ps}$, is applied at $\tau = 10.5\text{ps}$. Again, as in Fig. 3a, the numerical and analytical solutions practically coincide. In this case, the period of oscillations is large, $T = 2\pi/\gamma|\mu| \approx 126\text{ps}$, and the oscillations are not revealed.

Our results demonstrate that the analytical solutions represent a good approximation of the exact numerical solutions for both weakly and strongly coupled dimers (up to the values, $\epsilon \approx \pi/3$), for finite widths of π -pulses, and for both weak ($\eta \ll 1$) and strong ($\eta \gtrsim 1$) noises.

In Figs. 4a and 4b, N relatively wide π -pulses (with $\delta = 1\text{ps}$) were applied, with a distance between pulses, $\Delta = 1\text{ps}$. The dimer was chosen weakly coupled: $\epsilon \approx 0.17$. In Fig. 4a, the noise is weak ($\eta \approx 0.49$), and $N = 20$. In Fig. 4b, the noise is strong ($\eta \approx 1.97$), and $N = 10$. In this case, the value of the param-

eter, $\mu \approx 1.7i$, is imaginary, and one can observe the oscillations of $|\langle m(t) \rangle|$, with the period, $T/2 = \pi/\gamma|\mu| \approx 3.7$. Initially, the Bloch vector was oriented along the x -axis. During the initial time, $\tau = 1\text{ps}$, the Bloch vector experiences the FI decay. The first π -pulse was applied at $t = 1\text{ps}$. The FI decay is represented by the blue curves. The red curves demonstrate the evolution of the transverse component of the Bloch vector, under the influence of the π -pulses. As one can see, a significant improvement of the signal can be achieved.

IV. SIMULTANEOUS ACTION OF THE HOMOGENEOUS AND INHOMOGENEOUS DISORDER

Here, in addition to dynamical fluctuations (noise, $\xi(t)$), we consider an ensemble of TLSs (dimers) with fluctuating parameters, (Ω, θ, ϕ) , due to the static disorder. It is well-known that this leads to the inhomogeneous broadening of the FI signal decay. In our numerical simulations we assumed the independent Gaussian disorder for parameters, (Ω, θ, ϕ) . Our numerical simulations demonstrate that the main contribution from the static disorder, for a wide range of parameters, is due to the fluctuations of the frequency, Ω . So, below we neglect the static fluctuations of both angles, θ and ϕ . We assume a Gaussian distribution for the random parameter Ω , denoting the dispersion by σ_* . Note that the results can easily be extended by including the static fluctuations of angles, θ and ϕ , in the numerical solutions of the exact Eqs. (4) and (5).

In Fig. 5, we compare the results for the decay of the FI signal for three values of the dispersion, $\sigma_* = 0, 10, 20$, of static fluctuations of the frequency, Ω , and for the amplitudes of noise, $v = 20, 40$. The parameter, $\eta \approx 1.13$, so the noise is strong in this case. In the inset, oscillations are observed with the period, $T = 2\pi/\gamma|\mu|$, due to the imaginary value of the parameter, μ .

The analytical solution, which includes the contributions from both, the static disorder and the dynamical noise, and corresponds to the spin echo signal applied at the time τ , can be

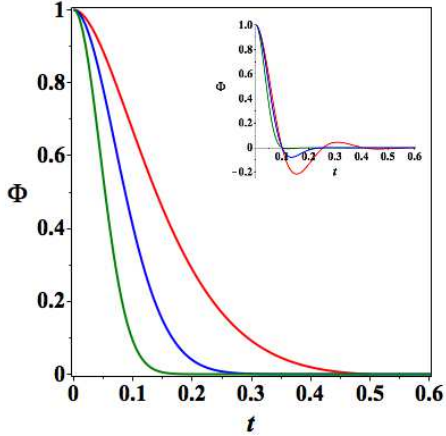


FIG. 5: (Color online) Simultaneous action of homogeneous and inhomogeneous broadening on the FI decay. The time dependence (in ps) of the generating functional, $\Phi(t)$. Red curve: $\sigma_* = 0$. Blue curve: $\sigma_* = 10$. Green curve: $\sigma_* = 20$. Parameters: $\Omega = 127$, $\theta = 0.968$, $\gamma = 10$, $v = 20$. Inset: $v = 40$.

written as, $\langle m(t) \rangle = \Phi_g^e(t) \langle m(0) \rangle$, where

$$\Phi_g^e(t) = \begin{cases} e^{-\frac{\sigma_*^2 t^2}{2}} \Phi^f(t), & 0 < t < \tau \\ e^{-\frac{\sigma_*^2 (t - 2\tau)^2}{2}} \Phi_g^f(t), & t > \tau. \end{cases} \quad (15)$$

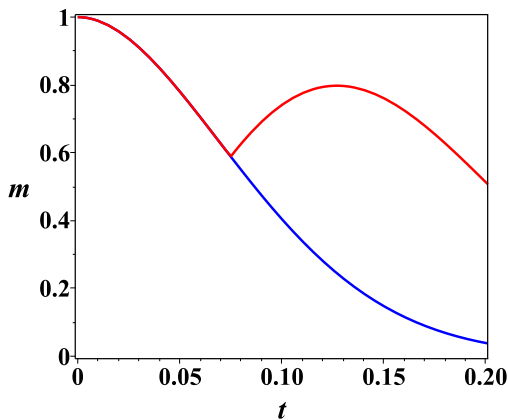


FIG. 6: (Color online) The decay of the FI signal in the presence of both homogeneous and inhomogeneous broadening (blue curve), and the action of the echo signal (red curve). Time dependence (in ps) of $m = |\langle m(t) \rangle|$. Parameters: $\Omega = 127$, $\theta = 0.968$, $\gamma = 10$, $v = 20$, $\sigma_* = 10$, $\tau = 0.075$.

In Fig. 6, both static disorder of Ω and the dynamical noise, $\xi(t)$, are included. The de-

cay of the FI signal is shown by the blue curve. For our chosen parameters, the FI signal decays in approximately 200fs. The spin echo signal was applied at $\tau = 75$ fs. As one can see, the echo pulse restores significantly the FI decay (red curve). Note that for the parameters chosen in Fig. 6, both dimensionless decay factors coincide at the characteristic time of the FI decay, $t_* = 200$ fs: $\gamma t_* = \sigma_*^2 t_*^2 / 2 = 2$. So, both homogeneous and inhomogeneous broadening are partly compensated in this case by the spin echo signal.

V. CONCLUSION

We presented the analytical and numerical results for the Hahn spin echo pulses for the two-level systems (TLSs) – chlorophyll-based dimers in bio-complexes, embedded in noisy protein environment. We have shown that even strong *dynamical* broadening can be suppressed significantly by the Hahn spin echo pulses. This is important for many bio-applications at ambient conditions. We also demonstrated the restoration of the free induction decay signal by the Hahn spin echo pulses when both homogeneous and inhomogeneous broadening equally contribute to the free induction decay. We recognize that in real experiments with bio-material, the application of the Hahn spin echo pulses may not correspond to the optimal protocol. So, different modifications of the considered here protocols will be needed. At the same time, the characteristic effects of the spin echo pulses for both weakly and strongly couple dimers and for weak and strong noises can be analyzed by using considered here simple protocols. Note, that the approach considered here is not a perturbative one, and it does not require any additional simplifications related to small parameters and different uncontrolled approximations. We also would like to mention here that the exact and closed system of equations which we derived for the Hahn echo protocols is a linear one. So, this system possesses the scaling properties, which are very useful, especially when performing the numerical simulations. Indeed, one can choose, for example, the “unreal” (short) pulses, and than easily apply the results for the “real” scaled parameters. We demonstrated these scaling properties of our approach both analytically and numerically.

The application of the spin echo technique is especially useful for bio-systems with strong

low-frequency dynamical noise, such as $1/f$ noise [12]. Our approach can be generalized for this case, as was done in [8], by introducing the corresponding ensemble of the fluctuators. Also, many different sources of dynamical noises can be included in the presented here approach (as was done in [22]).

Acknowledgments

This work was carried out under the auspices of the National Nuclear Security Administra-

tion of the U.S. Department of Energy at Los Alamos National Laboratory under Contract No. DE-AC52-06NA25396. A.I.N. acknowledges the support from the CONACyT, Grant No. 15349. G.P.B. acknowledges the support from the LDRD program at LANL.

-
- [1] M. Mohseni, Y. Omar, G.S. Engel, and M.B. Plenio (Eds.), *Quantum Effects in Biology*, (Cambridge University Press, 2014).
- [2] H. Dong and G.R. Fleming, *J. Phys. Chem. B*, **118**, 8956 (2014).
- [3] E.L. Hahn, Spin echoes, *Phys. Rev.*, **80**, 580 (1950).
- [4] R.J. Abraham, J. Fisher and P. Loftus, *Introduction to NMR spectroscopy*, (Wiley, Chichester, 1988).
- [5] G. Ithier, E. Collin, P. Joyez, P. J. Meeson, D. Vion, D. Esteve, F. Chiarello, A. Shnirman, Y. Makhlin, J. Schrieffer, and G. Schön, *Phys. Rev. B*, **72**, 134519 (2005).
- [6] J. Bergli, Y.M. Galperin, and B.L. Altshuler, *New Journ. Phys.* **11**, 025002 (2009).
- [7] Y.M. Galperin, B.L. Altshuler, J. Bergli, D. Shantsev, and V. Vinokur, *Phys. Rev. B*, **76**, 064531 (2007).
- [8] A.I. Nesterov and G.P. Berman, *Phys. Rev. A*, **85**, 052125 (2012).
- [9] M. Mohseni, P. Rebentrost, S. Lloyd, and A. Aspuru-Guzik, *J. Chem. Phys.*, **129**, 174106 (2008).
- [10] D. Xu and K. Schulten, *Chem. Phys.*, **182**, 91 (1994).
- [11] M. Merkli, G.P. Berman, and S.T. Sayre, *J. Math. Chem.*, **51**, 890 (2013).
- [12] T.G. Dewey and J.G. Bann, *Biophys. J. Biophys. Society*, **63**, 594 (1992).
- [13] M. Pudlak, *Physica A*, **341**, 444 (2004).
- [14] M. Pudlak, K.N. Pichugin, R.G. Nazmitdinov, and R. Pincak, *Phys. Rev. E*, **84**, 051912 (2011).
- [15] A.I. Nesterov, G.P. Berman, and A.R. Bishop, *Fortschritte der Physik*, **61**, 95 (2013).
- [16] J.M. Moix and J. Cao, *J. Chem. Phys.*, **139**, 134105 (2013).
- [17] F. Bloch. *Phys. Rev.*, **105**, 1206 (1957).
- [18] A.G. Redfield, *IBM J. Res. Dev.* **1**, 19 (1957).
- [19] M. Yang and G.R. Fleming, *Chem. Phys.*, **275**, 355 (2002).
- [20] V. Klyatskin, *Dynamics of Stochastic Systems*, (Elsevier, 2005).
- [21] F. Bretenaker and N. Treps (Eds.), *Laser: 50 Years of Discoveries*, (World Scientific Publishing Company, 2015).
- [22] A.I. Nesterov and G.P. Berman, *The role of protein fluctuation correlations in electron transfer in photosynthetic complexes*, arXiv:1412.0512 (2014)(To appear in *Phys. Rev. E*).